Peculiar supersolid phases induced by frustrated tunneling in the extended Bose-Hubbard model

Shao-Jun Dong, Wenyuan Liu, Xiang-Fa Zhou,[*] Guang-Can Guo, Zheng-Wei Zhou, Yong-Jian Han,[†] and Lixin He[‡]

Key Laboratory of Quantum Information, Chinese Academy of Sciences, University of Science and Technology of China, Hefei, 230026, China
and Synergetic Innovation Center of Quantum Information and Quantum Physics, University of Science and Technology of China, Hefei, 230026, China

By using a state-of-the-art tensor network state method, we study the ground-state phase diagram of an extended Bose-Hubbard model on the square lattice with frustrated next-nearest-neighbor tunneling. In the hard-core limit, tunneling frustration stabilizes a peculiar half-supersolid phase with one sublattice being superfluid and the other sublattice being Mott insulator away from half filling. In the soft-core case, the model shows very rich phase diagrams above half filling, including three different types of supersolid phases depending on the interaction parameters. The considered model provides a promising route to experimentally search for a novel stable supersolid state induced by frustrated tunneling in the region below half filling with dipolar atoms or molecules.

I. INTRODUCTION

The investigation of frustrated systems [1] has received sustained attention in the past due to its intimate association with different branches of condensed matter physics. The competition in frustrated systems usually greatly enriches the phase diagrams and leads to various exotic quantum phases, such as quantum spin liquids [2,3], magnetic domain patterns [4], and high-T_c superconductivity [5,6]. Recently, the experimental success of mimicking various theoretical models using ultracold atoms [7–10] provides a new platform to study the physics of the frustrated systems in a highly controllable manner. For instance, the frustrated Bose-Hubbard model can emerge when rotating optical lattices in the tight-binding limit, or with the help of synthetic gauge fields imposed by lasers [11]. These frustrated systems simulated by the neutral particles [12–23] offer great opportunities to explore new quantum phases.

Experimental searching for the supersolid (SS) phases is a longstanding challenge and has also received great attention recently. SS phases are characterized by the simultaneous appearance of crystalline and superfluid orders. Although its existence in ^{4}He was predicted a long time ago [24–26], experimental observation of the SS remains elusive [27]. Ultracold atoms offer another promising way; it is widely believed that SS can be stabilized in the extended Bose-Hubbard (EBH) model, which can be experimentally realized by loading dipolar bosons [28–31] into an optical lattice. It has been shown that a stable SS phase can exist in the geometrically frustrated triangular lattice [32–34]. However, in the square lattice, the SS phase becomes fragile resulting in the phase separation (PS) in the hard-core limit [35–41], especially when the filling factor $\rho < 1/2$, where the SS phase is missing or only takes a very narrow parameter range irrespective of anisotropic hoppings and interactions [42–44]. How the tunneling frustration changes the SS physics remains largely unexplored because the standard quantum Monte Carlo method may suffer from the sign problem.

In this work, we investigate an EBH model with frustrated next-nearest-neighbor (NNN) tunneling on square lattices. We calculate the ground states of the model via a state-of-the-art tensor network state (TNS) method. We identify a peculiar half-SS (HSS) phase that is stable in a large parameter space, where superfluid (SF) and Mott insulator (MI) are simultaneously supported within different sublattices away from half filling due to the presence of NNN hopping and nearest-neighbor (NN) repulsion V. Increasing the NNN tunneling can enlarge the portion of the HSS phase in the phase diagram, which appears even with very small filling factors. This is very different from the nonfrustrated case, where stable SS is always missing in this limit. In the soft-core case, the model shows very rich phase diagrams for $\rho > 1/2$, including three different types of SS states depending on the relative strength of different interaction parameters.

II. MODEL AND METHODS

The Hamiltonian considered in the paper reads,

$$H = -t_1 \sum_{\langle i,j \rangle} (b_i^\dagger b_j + h.c.) - t_2 \sum_{\langle\langle i,k \rangle\rangle} (b_i^\dagger b_k + \text{H.c.})$$
$$+ \frac{U}{2} \sum_i n_i(n_i - 1) + V \sum_{\langle i,j \rangle} n_i n_j, \tag{1}$$

where $\sum_{\langle i,j \rangle}$ and $\sum_{\langle\langle i,j \rangle\rangle}$ denote the summation of the nearest-neighbor (NN) and the next-nearest-neighbor (NNN) sites with hopping amplitude t_1 and t_2, respectively, $n_i = b_i^\dagger b_i$ is the number operator for boson. U is the on-site interaction energy, V denotes the interaction between NN sites. Without loss of generality, we assume $t_1 = 1$. When $t_2 < 0$, the model shows frustration effects.

The nonfrustrated EBH model has been extensively studied using both theoretical and numerical methods [35–37]. It has also been shown that in triangular lattices [32–34], the geometric frustration can stabilize the SS states. However, the previously studied systems have no tunneling frustration, and therefore can be reduced to nonfrustrated models [45]. Only a few studies concentrate on the corresponding SS physics with frustrated tunneling [21,45–47], since the standard quantum Monte Carlo simulation suffers from the notorious sign problem, which prevents a detailed numerical investigation.

―――――――
[*]xfzhou@ustc.edu.cn
[†]smhan@ustc.edu.cn
[‡]helx@ustc.edu.cn

We investigate the EBH model via a tensor network state (TNS) method [48–50], in which the many-particle wave functions can be represented by the products of tensors. The TNS wave functions are unbiased and are systematically improvable by increasing bond dimensions D. The method is free of the sign problem and therefore ideal for the frustrated EBH model. In this work, we use a special TNS, known as the string-bond state (SBS) [50]. More details of the method can be found in Ref. [51] and in Appendix A. We simulate the EBH model on a 10×10 square lattice with periodic boundary condition. We use the virtual bond dimension for the tensors up to $D = 10$, which converges the total energies with errors less than 10^{-2} per site for the phase separation states, and 10^{-3} per site for other phases.

III. RESULTS

A. Numerical results in the hard-core limit

To verify our method, we first reproduce the phase diagram for the case of $t_2 = 0$, which has been extensively investigated by QMC [35–37]. Our results are in good agreement with the previous QMC results (see Appendix B). Particularly, both QMC and our results show that in the hard-core limit, doping $\rho = 1/2$ with additional particles or holes leads to phase separation, which is a mixture of SF and checkerboard crystal (CBC), instead of a SS state.

We then apply the TNS method to study the model with $t_2 < 0$. Figure 1 shows a typical phase diagram of hard-core boson with frustrated $t_2 = -0.3$ in the ρ-V plane for $\rho \leqslant 0.5$. The phase diagram has a mirror symmetry about $\rho = 0.5$, because of the particle-hole symmetry. The most drastic change of the phase diagram is that a nontrivial half-SS (HSS) phase
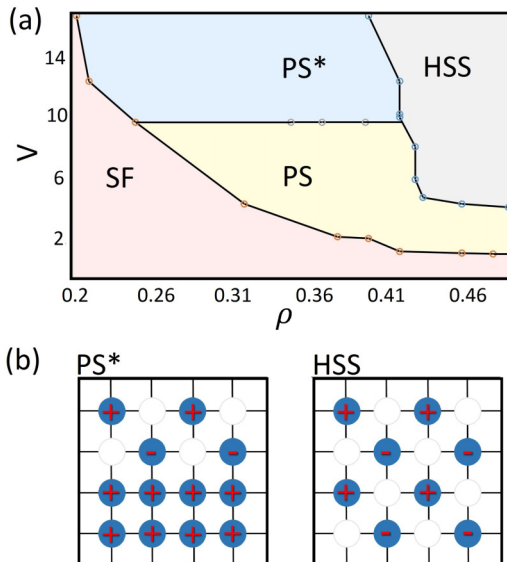

FIG. 1. (a) The ground-state phase diagram of the frustrated EBH model in the hard-core limit with $t_2 = -0.3$. Four phases have been identified including a superfluid (SF) phase, a half-supersolid (HSS) phase, phase separation (PS) consisting of SS and SF, and PS* consisting of SF and HSS. (b) The schematic plot of the on-site $\langle n_i \rangle$ for the HSS and PS* state. The empty circles represent $\langle n_i \rangle = 0$. The $\pm$ signs in the blue circles indicate the on-site boson phase $\arg[\langle b_i \rangle]$.

with the checkerboard pattern emerges at $\rho \in (0.4, 0.5)$ and $V > 3$, compared to the phase separation regime in the $t_2 = 0$ case. The presence of t_2 provides another hopping channel to lower the energy of the system for doped holes (particles) within the occupied (unoccupied) sublattice. Since t_2 hopping only happens within one sublattice, the checkerboard pattern is preserved. This is very different from the $t_2 = 0$ case, where doped holes form a planar domain wall due to NN hopping t_1, which destroys the uniform CBC background and results in phase separation.

To illustrate the nontrivial properties of such a HSS phase, we schematically show the on-site boson density $\langle n_i \rangle = \langle b_i^\dagger b_i \rangle$ of the HSS phase in Fig. 1(b), in which $\langle n_i \rangle$ forms two sublattices (the detailed numerical results are given in Appendix B). Interestingly, in one of the sublattices both $\langle n_i \rangle$ and $\langle \delta n_i \rangle$ are uniformly distributed, which corresponds to a uniform SF phase, and the other sublattice is either fully unoccupied ($\rho < 1/2$) or occupied ($\rho \geqslant 1/2$) with one particle per site, which is precisely a MI. Since the two interlaced sublattices result in a checkerboard-type density distribution, the whole system possesses both crystalline and SF orders, and can be viewed as some kind of SS phase. However, the simultaneous existence of SF and MI phases in different sublattices makes it very different from traditional checkerboard SS in the lattice, in which both sublattices have SF order but with different densities. Since SF order exists only within one sublattice, we call this phase a HSS.

The HSS phases are further distinguished from usual SS phases by their nontrivial phase patterns $\arg[\langle b_i \rangle]$, as shown in Fig. 1(b). The HSS phase is composed of the equal superposition of two strip orders with $\vec{k} = (\pi, 0)$ and $(0, \pi)$. For each site i in the MI sublattice, the summation $\sum_{\bar{i}} \langle b_{\bar{i}} \rangle$ over all NN sites within the SF sublattice vanishes due to the phase patterns shown in Fig. 1(b). There is no net particle tunneling between the two sublattices even in the presence of the nonvanishing NN hopping t_1, and therefore, the MI sublattice is stabilized even away from half filling.

The PS* phase in Fig. 1 consists of both the HSS phase and the SF phase that are separated in the real space, as schematically shown in Fig. 1(b). The phase boundaries between the SF and HSS are determined by the real-space distribution of $\langle n_i \rangle$ and $\langle \delta n_i \rangle$ shown in Appendix B. In the SF region, both $\langle n_i \rangle$ and $\langle \delta n_i \rangle$ distribute almost uniformly, in sharp contrast with the HSS region. The usual PS (CBC+SF) appears only when V is small. In addition, there exists a direct first-order transition from PS to HSS. This is somehow different from the mean-field treatment, where the PS* is always sandwiched between them as shown in Appendix C. Within numerical precisions, the critical point ($V_c = 10$) between PS and PS* is almost independent of the filling factor ρ, which is consistent with the mean-field predictions discussed in Appendix C.

To further characterize the properties of the different phases, we calculate the static structure factor at $\vec{k} = (\pi, \pi)$ as

$$S_n(\vec{k}) = \frac{1}{M} \sum_{i,j} \langle n_i n_j \rangle e^{-i\vec{k} \cdot (\vec{r}_i - \vec{r}_j)}, \qquad (2)$$

which can be used to identify the diagonal long-range order in the system. Here M is the total number of lattice sites. The SF
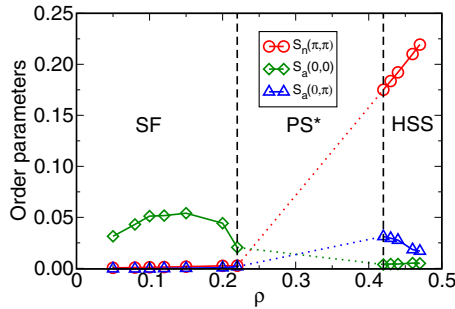
FIG. 2. Order parameters $S_n(\pi,\pi)$, $S_a(0,0)$, and $S_a(0,\pi)$ as functions of the filling factor ρ at $V = 12$ and $t_2 = -0.3$ in the hard-core limit. The system shows SF to PS* and PS* to HSS phase transitions as ρ increase from 0–0.5.

orders are measured by the correlation function defined by

$$S_a(\vec{k}) = \frac{1}{M} \sum_{i,j} \langle b_i^\dagger b_j \rangle e^{-i\vec{k}\cdot(\vec{r}_i - \vec{r}_j)}. \qquad (3)$$

While generally the SF phase is characterize by the sharp peak of $S_a(\vec{k})$ around $\vec{k} = (0,0)$, SS phase is identified by the presence of both $S_a[\vec{k} = (0,0)]$ and $S_a[\vec{k} = (\pi,\pi)]$ accompanied by a nonzero structure factor $S_n[\vec{k} = (\pi,\pi)]$, which indicates a crystal order. The HSS phase has equal $S_a(\vec{k})$ around $\vec{k} = (\pi,0)$ and $(0,\pi)$ along with the presence of the long-range density wave order as explained previously, especially when $\rho > 1/2$, the occupied MI sublattice induces a strong background signal to all $S_a(\vec{k})$, which clearly discriminates such peculiar HSS states from the usual checkerboard SS phase.

Figure 2 displays the calculated order parameters $S_n(\vec{k})$ and $S_a(\vec{k})$ of the ground state as a function of ρ for fixed $V = 12$ and $t_2 = -0.3$. When the filling factor ρ is small, the ground state is a SF characterized by nonzero $S_a(0,0)$ and vanishing $S_n(\pi,\pi)$. Increasing ρ across a critical value ($\rho \approx 0.2$), SF is unstable towards an intermediate PS* region composed of HSS and SF. For $\rho \geqslant 0.4$, the SF component disappears, and the system becomes a uniform HSS state with nonzero $S_n(\pi,\pi)$ and $S_a(\pi,0)$ [and $S_a(0,\pi)$]. Approaching half filling, all the order parameters $S_a(\pi,0)$ [and $S_a(0,\pi)$] vanish except $S_n(\pi,\pi)$, which corresponds to the CBC phase.

To see if the HSS phase is stable in the thermodynamic limit, we calculate the order parameters $S_a(0,0)$, $S_a(0,\pi)$, and $S_n(\pi,\pi)$ with $t_2 = -0.3$, $V = 12$, on the $L \times L$ lattices, where $L = 6, 8, 10, 12$, at $\rho \approx 0.46$, and perform finite-size scaling. The results are shown in Figs. 3(a), 3(b), and 3(c), respectively. As $L \to \infty$, we have $S_a(0,0) = 0$, whereas both $S_a(0,\pi)$ and $S_n(\pi,\pi)$ are finite. These results suggest that the HSS phase is indeed stable in the thermodynamic limit.

To show how the presence of frustration, t_2, affects these phases, we also plot the phase diagram in the t_2-ρ plane for fixed $V = 16$, as shown in Fig. 4. For small t_2, PS appears immediately as we dope the crystal at $\rho = 1/2$ with holes. Increasing t_2 makes it more energetically favorable for the additional holes hopping within the occupied sublattice to form the uniform HSS. Meanwhile the usual PS is replaced with PS* when $|t_2| \geqslant 0.24$. The calculation indicates that HSS should dominate the phase diagram while the PS* region shrinks as we
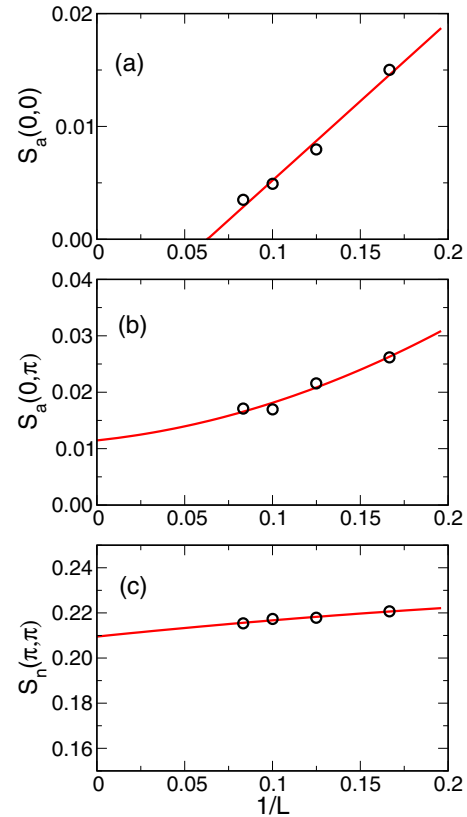

FIG. 3. The order parameters (a)$S_a(0,0)$, (b) $S_a(0,\pi)$, and (c) $S_n(\pi,\pi)$ as functions of $1/L$, for $L = 6, 8, 10, 12$, with $t_2 = -0.3$, $V = 12$, and $\rho \approx 0.46$. As $L \to \infty$, $S_a(0,0) = 0$, whereas both $S_a(0,\pi)$ and $S_n(\pi,\pi)$ are finite, suggesting that the HSS phase is stable in the thermodynamic limit.

approach the critical point at $|t_2| = t_1/2$. This is very different from the nonfrustrated case, where stable SS is missing for $\rho < 1/2$ even for the soft-core case. Therefore introducing the frustration hopping term is a promising route to observe the (H)SS phase.

B. SS phases in the soft-core case

When going beyond the hard-core limit, the EBH model shows far more rich phase diagrams depending on the values of the on-site interaction strength U. In the absence of NNN hopping, previous results show that doping $\rho = 1/2$ with
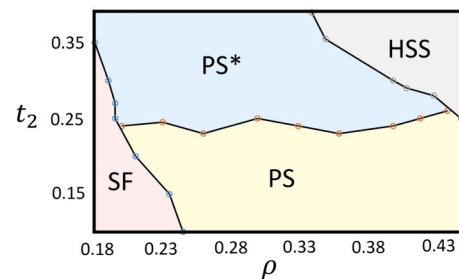

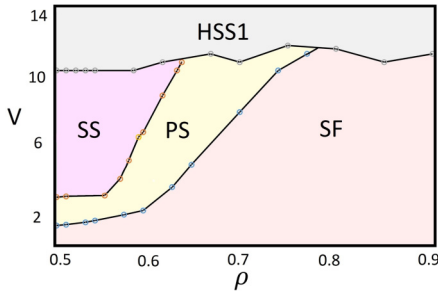FIG. 4. The ground-state phase diagram of the hard-core frustrated EBH model in the t_2-ρ plane, with $V = 16$.

FIG. 5. The ground-state phase diagram of the soft-core frustrated EBH model in the ρ-V plane with $t_2 = -0.3$ and $U = 40$.

FIG. 6. The order parameters $S_a(\pi,0)$ as functions of U at $t_2 = -0.3$, $\rho = 0.55$, for different ratios $zV/U = 0.8$ and 0.5 respectively.

additional particles may lead to a stable SS phase [37]. The key issue here is how this general picture changes due to the presence of HSS phase for $t_2 \neq 0$.

Intuitively, when $2\Delta = zV - U \sim 0$, the doped particles can be placed on either of the two sublattices due to the vanishing energy difference. Therefore, particles can hop around the whole lattice due to NN hopping, which results in the usual checkerboard SS. When $\Delta < 0$, it is more energetically favorable for the additional particles to occupy the empty sublattice, while the other one remains to be a MI. This indicates that the HSS state discussed above should be more robust for large U, and is consistent with those discussed in the hard-core limit. For $\Delta > 0$, the additional particles tend to locate on the occupied lattice site while the empty sublattice remains unchanged. Therefore, there should also exist another kind of HSS phase (HSS1) in this limit (see Appendix C for details).

Figure 5 depicts the phase diagram with a constant on-site interaction $U = 40$ and $t_2 = -0.3$. The result for $\rho < 0.5$ is almost the same as the hard-core limit, and therefore is not shown. For these parameters, a stable conventional SS does exist whereas the HSS phase completely disappears above the half filling. The PS* phase consisting of HSS and SF is also missing for parameters we used here. However, the region of SS phase is greatly shrunk due to $t_2 \neq 0$ compared with usual extended BH model. Moreover, the PS regime extends up to the critical line $zV = U$, and is sandwiched between SS and SF phases. When the filling factor $\rho \to 1$, the system is a SF state below the critical line $zV = U$. Above $zV > U$, a new HSS1 phase dominates the phase diagram for all ρ. HSS1 is different from the HSS state in the $\rho > 0.5$ region, which has particle-hole symmetry to the HSS state in the $\rho < 0.5$ region, i.e., it has one sublattice that is fully occupied by one boson per site, without fluctuation, and the other sublattice is SF. The HSS1 also have two sublattices with one sublattice being unoccupied, and the other one being SF with the occupation number larger than one per site. Interestingly, there is a MI transition in one sublattice going from the SS phase to the HSS or the HSS1 phases.

To see how the HSS phase that presented in the hard-core limit disappears at $U = 40$, we show in Fig. 6 the order parameters $S_a(\pi,0)$ as functions of U for different ratios $zV/U = 0.8$ and 0.5 respectively at $\rho = 0.55$. At large U, the HSS phase does exist, but it undergoes a transition to the SS state as U decreases. The transition from HSS to SS is located
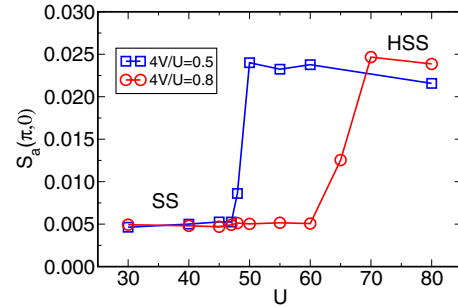
at $U \sim 50$ for $zV/U = 0.5$ and $U \sim 65$ for $zV/U = 0.8$. The SS and HSS phases can coexist in the phase diagram for $U \in (50,60)$. These results suggest that for a given U, the region with larger V will become SS state first, whereas the region with smaller V can still be HSS. When $U = 40$, the SS-HSS transition may happen at a rather small V. However, in this case, a PS phase would be more stable, and therefore no HSS phase appears in Fig. 5.

IV. DISCUSSION

Experimentally, frustrated NNN hopping can be realized using spin-dependent lattice via Raman process, as demonstrated in Ref. [22]. The effective NN repulsion can be implemented using dipolar bosons [29–31] or molecules with tunable ratio V/U via Feshbach resonance. Finally, the predicted phases can be identified from their typical density and momentum distributions shown in Table I, which can be detected using the time-of-flight (TOF) imaging method combined with the *in situ* detections.

V. SUMMARY

We have studied the phase diagram of the extended Bose-Hubbard models with frustrated hoppings via the TNS method. We show that a peculiar HSS phase can be stabilized below half filling even in the hard-core limit, which is absent from the usual nonfrustrated Bose-Hubbard models. For the soft-core model, the competition of on-site interaction and frustration leads to different types SS phases above half filling. The frustrated models proposed here can be implemented in current experimental systems with no fundamental challenge. In this work we focus on the case $|t_2| < t_1/2$, but it would

TABLE I. Characteristic order parameters for different supersolid phases discussed in the paper, where $\vec{k}_0 = (0,0)$, $\vec{k}_1 = (\pi,0)$, $\vec{k}_2 = (0,\pi)$, and $\vec{k}_3 = (\pi,\pi)$. S_a' describes the background noise for all $\vec{k}$ due to the presence of Mott-insulator sublattice above half filling.

	HSS ($\rho < \frac{1}{2}$) or HSS1	HSS ($\rho > \frac{1}{2}$)	SS
$S_a(\vec{k})$	$S_{a,\vec{k}_1} = S_{a,\vec{k}_2} \neq 0$	$S_{a,\vec{k}_1} = S_{a,\vec{k}_2} \neq 0$, and $S_a' = \frac{1}{2}$	$S_{a,\vec{k}_0} \neq 0$ $S_{a,\vec{k}_3} \neq 0$
$S_n(\vec{k})$	$S_{n,\vec{k}_0} = S_{n,\vec{k}_3} \neq 0$	$S_{n,\vec{k}_0} \neq 0$ $S_{n,\vec{k}_3} \neq 0$	$S_{n,\vec{k}_0} \neq 0$ $S_{n,\vec{k}_3} \neq 0$

be interesting to see how these predicted phases change when approaching the limit $|t_2| \sim t_1/2$, where a spin-liquid state is predicted to exist.

APPENDIX A: STRING-BOND STATE METHOD

Recently developed tensor network states (TNS) methods, including the matrix product states (MPS) [48,52,53], the projected entangled pair states (PEPS) [49], string-bond states (SBS) [50], and the multiscale entanglement renormalization ansatz (MERA) [54], etc. provide a promising scheme to solve the longstanding quantum many-body problems. In this scheme, the variational space can be represented by polynomially scaled parameters instead of exponential ones. Once we have the TNS representation of the many-particle wave functions, the ground-state energies, as well as corresponding wave functions, can be obtained variationally.

In this paper, we investigate the ground-state properties of the extended Bose-Hubbard model using SBS [50]. The wave functions represented in SBS form can be written as

$$|\Psi\rangle = \sum_{s_1 \cdots s_N} \prod_{p \in \mathcal{P}} \text{Tr}\left[\prod_{k \in p} A_{p,k}^{s_k} \right] |s_1 \cdots s_N\rangle, \qquad (A1)$$

where $\mathcal{P}$ is a certain string pattern, which contains a set of strings p. The product of matrices $A_{p,k}^{s_k}$ with virtual bond dimension D over $k \in p$ means over the sites k in the order appearing in the string p, and d is the dimension of the physical indices s_k on site k. In this case, d is the possible boson occupation number at each site. We use $d = 2$ for the hard-core boson, and $d = 4$ in the soft core case (i.e., the maximum allowed boson on each site is 3). We use two long strings as shown in Fig. 7. This type of SBS satisfies area law [50,55], and the results can be systematically converged by increasing the bond dimension D.

For a given a Hamiltonian H, the total energy of the system is a function of the tensors at each lattice site $A_{p,k}^{s_k}$, i.e., $E = E(\{A_{p,k}^{s_k}\})$. We recently developed an efficient algorithm to obtain the ground-state wave function and corresponding energy, by mapping the problem to optimizing the total energy of a classical mechanical system, in which the elements $a_{ij}^{s_k}(p,k)$ of the tensor $A_{p,k}^{s_k}$ are treated as the generalized coordinates of the system. The ground-state wave function and total energy is then obtained via a replica-exchange molecular dynamic simulation. Details of the method are presented in Ref. [51]. The replica-exchange (also known as parallel tempering) [56,57] MD method can effectively avoid the system being trapped in local minima, which is very
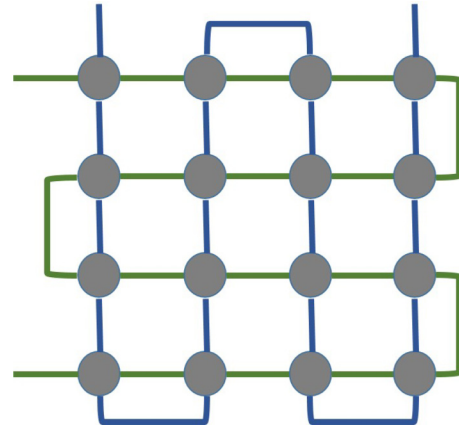

FIG. 7. The string-bond states (SBS) pattern used in the calculations, which is made up of two long strings.

important for accurate simulation of complex states such as phase separations.

In our simulations, we use $M = 48$ temperatures. Initially, the temperatures distribute exponentially between the highest ($1/\beta_0 = 0.01$) and lowest ($1/\beta_{M-1} = 10^{-6}$) temperatures. For each temperature, we start from random tensors. During the simulations, we adjust the temperatures after configuration exchange for ten times, whereas there are 300 MD steps between the two configuration exchanges, with a step length $\Delta t = 0.01$. For each MD step, we sample about 40000 configurations. The energies used for temperature exchange are averaged over 250 MD steps. After we finish the replica-exchange MD optimization, we further decrease the temperature to 10^{-7} to obtain more accurate results.

Figures 8(a), 8(b) show the convergence of total energy per site with increasing bond dimension D in for two typical parameter sets. When $D = 10$, the total energies converge to less than 10^{-2} per site for the phase separation states, and 10^{-3} per site for pure phases.

APPENDIX B: SOME DETAILED NUMERICAL RESULTS

1. Results for $t_2 = 0$ model

To benchmark our method, we first calculate the phase diagrams for $t_2 = 0$ model, which has no tunneling frustration, and compare the results to those obtained from quantum Monte Carlo (QMC) simulations for the hard-core bosons [36] and
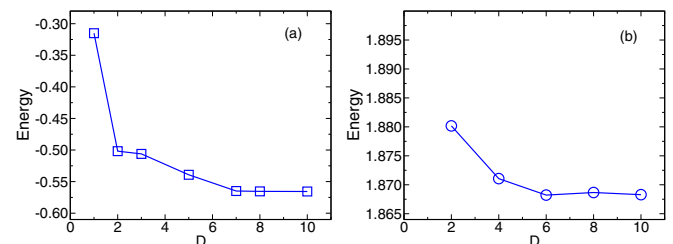

FIG. 8. The total energy per site as functions of bond dimension D for (a) the hard-core limit, with $V = 1$, $t_2 = -0.3$, $\rho = 0.32$, which is in the SF phase; and (b) the soft-core case with $U = 40$, $V = 12$, $t_2 = -0.3$, and $\rho = 0.55$, which is in the HSS1 phase.
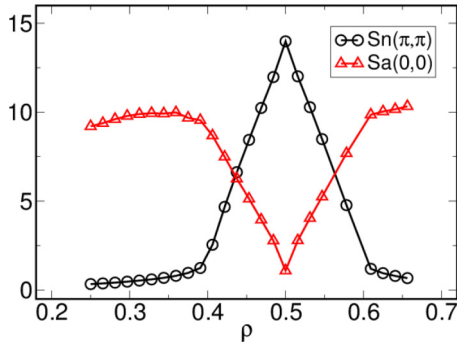
FIG. 9. The structure factors $S_n(\pi,\pi)$ and $S_a(0,0)$ as functions of density ρ for the $t_2 = 0$, $V = 3$ hard-core Bose-Hubbard model on a 8×8 lattice.

FIG. 10. The phase diagrams of the extended Bose-Hubbard model with $U = 20$, $t_2 = 0$ on 10×10 lattice in the V-ρ plane. We show only the region of $\rho > 0.5$. The red dashed lines are calculated by SBS method, whereas the black solid lines are extracted from Ref. [37]

soft-core bosons [37]. In Fig. 9, we plot the structure factors $S_n(\pi,\pi)$ and $S_a(0,0)$ as functions of filling density ρ for the hard-core model. The results are obtained on a 8×8 lattice with $V = 3$. The structure factors and phase boundaries obtained using the SBS are in good agreement with those obtained from QMC with the same parameters (see Fig. 1 of Ref. [36]). In Fig. 10, we compare the V-ρ phases diagrams for $\rho \geqslant 0.5$ with $t_2 = 0$, $U = 20$ on a 10×10 lattice calculated by the SBS method (red dashed lines) with those obtained from QMC method with the same parameters (black solid lines extracted from Ref. [37]), which have good agreement.

2. Density distribution and fluctuation of different phases

The various phases emerge from the frustrated EBH model can be distinguished from their density distributions $\langle n_i \rangle = \langle b_i^\dagger b_i \rangle$ and density fluctuations $\langle \delta n_i \rangle$ in real space. We show in Fig. 11 the typical on-site density distribution $\langle n_i \rangle$ (top panel) and corresponding density fluctuation $\langle \delta n_i \rangle$ (bottom panel) for the frustrated Bose-Hubbard model in the hard-core limit and filling $\rho < 0.5$, including the superfluid (SF), half-supersolid (HSS), phase separation (PS), and PS* phases. The SF phase has almost uniformly distributed density $\langle n_i \rangle$ and so does the density fluctuation $\langle \delta n_i \rangle$ on each site. The HSS phase clearly shows two sublattices, with one sublattice fully
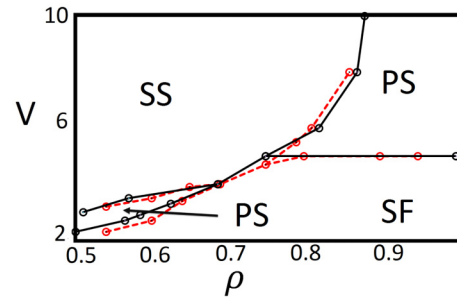
unoccupied and absent of $\langle \delta n_i \rangle$. The other sublattice is SS, with nonvanishing boson density and density fluctuation. The PS phase shows distinct regions in real space with one being SF, and the other being CBS, whereas in the PS* phase, there are also two distinct regions with one being SF, and the other being HSS.

Figure 12 shows the typical density distribution $\langle n_i \rangle$ (top panel) and corresponding density fluctuation $\langle \delta n_i \rangle$ (bottom panel) for the frustrated EBH model in the soft-core case and filling $\rho > 0.5$, including PS, SS, HSS, and HSS1 phases. The PS phase is composed of the SF and CBS phase. The SS phase clearly has both solid order and SF order. It has two sublattices, both have nonvanishing density distribution $\langle n_i \rangle$ and density fluctuation $\langle \delta n_i \rangle$ on each site, which is different from those of the HSS phase. In the soft-core case with $\rho > 0.5$, there are two HSS phase, namely HSS and HSS1. When $\rho > 0.5$, one of the sublattice of HSS is fully occupied, with occupation number equal one. The other sublattice is SF. This phase can be viewed as a particle-hole mirror image of the HSS phase for $\rho < 0.5$. The HSS1 phase also has two sublattices, but it is different from the HSS phase as it has one fully unoccupied sublattice, and the other one being SS with the occupation number larger than one.
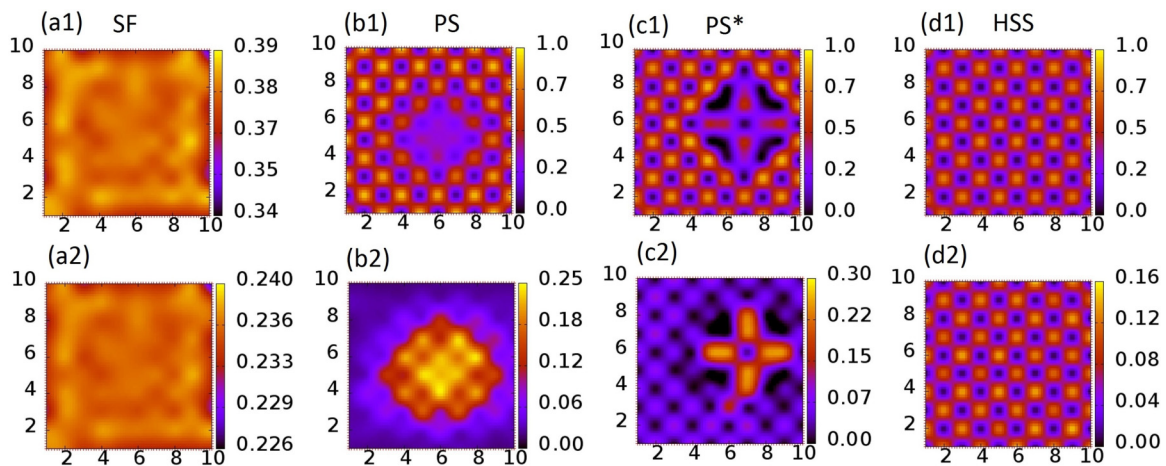

FIG. 11. Top: Typical boson density distribution $\langle n_i \rangle = \langle b_i^\dagger b_i \rangle$ for (a1) superfluid (SF), (b1) phase separation (PS), (c1) PS*, and (d1) half-supersolid (HSS) phases in the hard-core limit and filling $\rho < 0.5$. Bottom: (a2)–(d2) Corresponding density fluctuation $\langle \delta n_i \rangle$ for each phase.
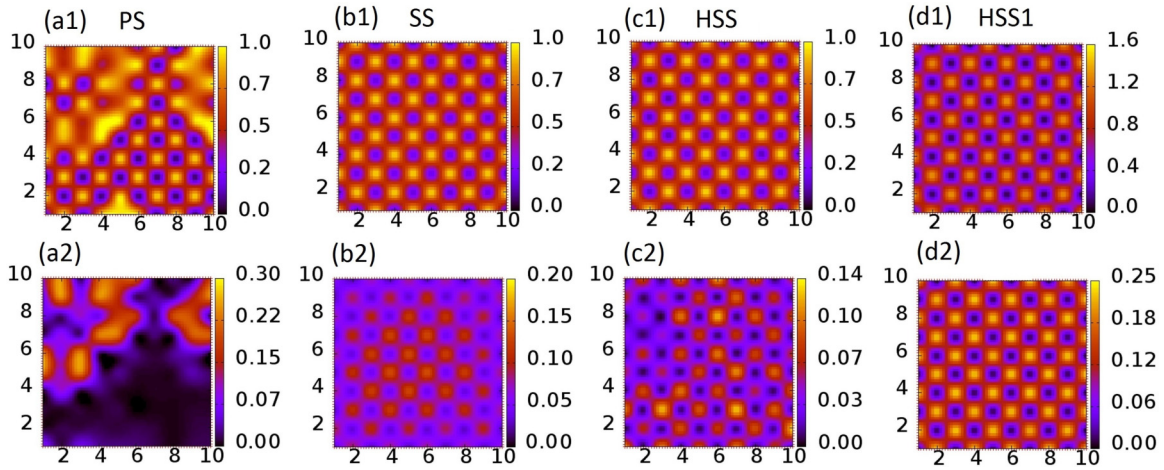
FIG. 12. Top: Typical boson density distribution $\langle n_i \rangle$ for (a1) PS, (b1) SS, (c1) HSS, and (d1) HSS1 phases in the soft-core case and filling $\rho > 0.5$. Bottom: (a2)–(d2) Corresponding density fluctuation $\langle \delta n_i \rangle$ for each phase.

APPENDIX C: RESULTS FROM MEAN-FIELD THEORY

Since the standard mean-field calculation cannot capture the main physics related to phase separation, we employ the method introduced by Kimura [58], which combines the Gutzwiller variational wave function and linear programming method. It has been proved that such method can effectively describe the phase diagram within a canonical ensemble with fixed total boson number, especially in the hard-core limit. Specifically, we assume the total free energy of the system can be written as the combination of two different phases $E_t = \gamma E_A + (1 - \gamma) E_B$ with γ the area ratio of phase A in the entire system. To obtain the ground state, we minimize E_t subject to the particle-number condition as $N_t = \gamma N_A + (1 - \gamma) N_B$. When $\gamma = 0$ or 1, the system stays in a uniform phase B or A without phase separation. While for $\gamma \in (0, 1)$, a mixture of phases A and B occurs, which indicates the existence of phase separation.

In the case of $t_2 = 0$, the corresponding phase diagram has been widely studied using standard quantum Monte Carlo method. The calculation shows that when $U/|t_1| \to \infty$, the supersolid state is unstable due to the presence of PS into a mixture of uniform SF and crystal. This is because away from half filling, the additional holes for $\rho < 0.5$ tend to to form a planar domain wall with the energy gain $\Delta E_1 \sim -ct_1$ per holes. While for an isolated hole, the kinetic energy gain is only estimated as $\Delta E_1' \sim -4t_1^2/3V$. This leads to the instability of the crystal phase at $\rho = 1/2$ when doped with holes, which finally develops into the mixture a uniform superfluid and the checkerboard solid. In the other limit with $t_1 = 0$, the presence of NNN hopping t_2 provides another channel to lower the energy of the system away from half filling. The additional holes can hop around the background of a checkerboard density wave with the energy gain determined by $\Delta E_2 \sim -4t_2$. In this case, the superfluid can exist for $\rho < 1/2$ accompany with a checkerboard density wave, which is the characteristic feature of supersolid (SS) phases. Since we have $t_2 < 0$, the interference effect ensures that particles only reside within one sublattice. Such half-SS (HSS) state is different from the usual SS state when $t_2 > 0$, where additional holes can jump between the two sublattices.

In the presence of both t_1 and t_2, the competition of above two mechanisms leads to a rich phase diagram in the ρ-V plane. The system can be in a HSS state or PS depending closely on the relative strength of t_1, t_2, and V respectively. The total energy gain of PS can be estimated as $\Delta E_1 \sim -ct_1 + dV$ taking into account the interaction between neighboring lattice sites. When both t_2 and V are comparatively small, the PS state has much lower energy, which excludes the possibility of SS state away from half filling. However, in the opposite case, we have $\Delta E_2 < \Delta E_1$, which indicates that the SS phase is stabilized by the NNN hopping and NN repulsive interaction. To obtain the boundaries of various phases, we employ a perturbation analysis using the canonical ensemble.

1. Phase separation into SF and HSS state from HSS

For relatively larger V, the presence of NNN hopping t_2 can stabilize the HSS phase away from half filling, where SF exists only within one sublattice. While in the opposite limit with $\rho \sim 0$ or $(1 - \rho) \sim 0$, a uniform SF state has much lower energy. It is expected that in the intermediate regime, there exists a PS* state composed of the mixture of the SF state and HSS state. This is very different from the normal case with $t_2 = 0$, where PS occurs immediately when the system is doped with additional holes or particles in the background of CB solid at half filling.

In the hard-core limit, we assume the Gutzwiller wave functions of HSS and SF phases to be

$$|\psi_{\text{hss}}\rangle = d_0 |0\rangle + d_1 |1\rangle, \text{ and } |\psi_{\text{sf}}\rangle = c_0 |0\rangle + c_1 |1\rangle.$$

The total number of particles per site can be expressed as

$$\rho = (1 - \gamma_{\text{sf}})(\rho - \delta\rho) - \gamma_{\text{sf}}\rho_{\text{sf}}, \tag{C1}$$

where we have set γ_{sf} the ratio of SF phase. The coefficients of wave functions $|\psi_{\text{hss}}\rangle$ and $|\psi_{\text{sf}}\rangle$ are related to the mean number of particles through $|d_0|^2 = 1 - |d_1|^2 = 2(\rho - \delta\rho)$ and $|c_0|^2 = 1 - |c_1|^2 = 1 - \rho_{\text{sf}}$. Near the transition boundary, we have $\delta\rho \simeq \gamma_{\text{sf}}(\rho_{\text{sf}} - \rho)$. The total variational energy of the system

is obtained as

$$E_t = (1 - \gamma_{\text{sf}})E_{\text{hss}} - \gamma_{\text{sf}}E_{\text{sf}}$$

$$\simeq 2zt_2(\rho - 2\rho^2) + \gamma_{\text{sf}}\{2[V + 2(t_1 + t_2)]\rho_{\text{sf}}^2$$

$$+ 4(-t_1 - (2 - 4\rho)t_2)\rho_{\text{sf}} + 8\rho^2 t_2\}. \quad \text{(C2)}$$

The transition point can then be found by setting the coefficient of γ_{sf} to be zero. This is achieved when $\rho_{\text{sf}} = 4\rho t_2/[4\rho t_2 - (t_1 + 2t_2)]$ for $t_1 + 2t_2 > 0$. The corresponding critical values of V and ρ are obtained as

$$V_c = -2t_2 - \frac{(t_1 + 2t_2)[t_1 + 2t_2 - 8t_2\rho(1 - \rho)]}{4\rho^2 t_2}, \quad \text{and}$$

$$\rho_c = \frac{(t_1 + 2t_2)}{2\sqrt{|t_2|}(\sqrt{V + 2t_1 + 2t_2} - 2\sqrt{|t_2|})}. \quad \text{(C3)}$$

Therefore, for given total number of particles per site, we have a HSS state for $V > V_c$ while PS occurs for $V < V_c$. The same argument applies to ρ_c, where PS phase appears when $\rho < \rho_c$ for fixed NN repulsive interaction V. In the case of half filling, we have $V_c = -2(t_1 + t_2) - t_1^2/t_2$.

2. PS into HSS and SF phases from SF

For larger NN repulsive interaction V, an increase of the total particle number leads to the transition from a SF state to the mixture of SF and HSS states. The boundary can also be obtained using a similar method discussed above. The constraint of total number of particles per site leads to

$$\rho = (1 - \gamma)(\rho - \delta\rho) + \gamma\rho_{\text{hss}} \quad \text{(C4)}$$

with γ and ρ_{hss} corresponding to the ratio and mean number of particles in HSS phase, respectively. The total variational energy of the system can be derived as

$$E_t = (1 - \gamma)E_{\text{sf}} + \gamma E_{\text{hss}}$$

$$= -z(t_1 + t_2)\rho(1 - \rho) + \frac{zV}{2}\rho^2$$

$$+ \gamma\frac{z}{2}\{A\rho^2 - 4t_2\rho_{\text{hss}}^2 - 2[A\rho - (t_1 + 2t_2)]\rho_{\text{hss}}\}$$

$$\text{(C5)}$$

with $A = V + 2(t_1 + t_2)$. Due to the internal symmetry, here we only concentrate on the case with $\rho \in [0, 1/2]$. Similar argument applies by replacing ρ with $(1 - \rho)$ when $\rho \in (1/2, 1]$.

The boundary can be solved by looking at the minimal of coefficient associated with γ

$$f(\rho_{\text{hss}}) = A\rho^2 - 4t_2\rho_{\text{hss}}^2 - 2[A\rho - (t_1 + 2t_2)]\rho_{\text{hss}}. \quad \text{(C6)}$$

Since phase separation occurs only when $f(\rho_{\text{hss}}) < 0$, the critical V_c and ρ_c can be obtained by setting $f(\rho_{\text{hss}}) = 0$ within the regime $\rho \in [0, 1/2]$. Generally, it is easy to check that $f(\rho_{\text{hss}})$ reaches its minimal

$$f(N_{\text{hss}})_{\text{min}} = A\rho^2 - 4|t_2|\rho_{\text{hss}}^2$$

when $\rho_{\text{hss}} = -[A\rho - (t_1 + 2t_2)]/4t_2$, which is less than $1/2$ only when $V > -2(t_1 + t_2) - t_1^2/t_2$. Setting $f(\rho_{\text{hss}})_{\text{min}} = 0$, we obtain $\rho_{\text{hss}} = (t_1 + 2t_2)/2(\sqrt{A|t_2|} - 2|t_2|)$. The corre-
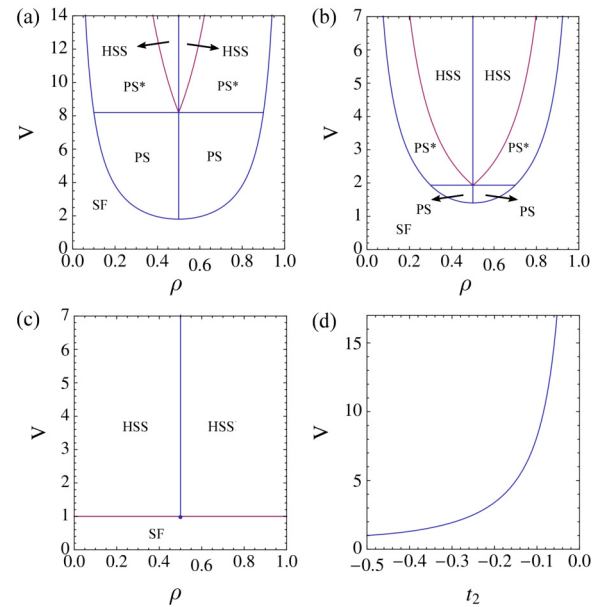

FIG. 13. Phase diagrams in the hard-core limit in the ρ-V plane for different (a) $t_2 = -0.1$, (b) $t_2 = -0.3$, and (c) $t_2 = -0.5$ with fixed $t_1 = 1$. (d) shows the critical $\widetilde{V}_c = -2(t_1 + t_2) - t_1^2/t_2$ as a function of t_1 and t_2.

sponding critical ρ and V read

$$\rho_c = \frac{t_1 + 2t_2}{A - 2\sqrt{A|t_2|}}, \quad \text{and}$$

$$V_c = \frac{1 - 2\rho}{\rho}(t_1 + 2t_2) + 2\sqrt{t_2\left(t_2 - \frac{t_1 + 2t_2}{\rho}\right)}. \quad \text{(C7)}$$

When $\rho_{\text{hss}} = 1/2$, the critical NN repulsive interaction reduces to $\widetilde{V}_c = -2(t_1 + t_2) - t_1^2/t_2$ with $\widetilde{\rho}_c = |t_2|/t_1$. When $V < -2(t_1 + t_2) - t_1^2/t_2$, $f(\rho_{\text{hss}})$ reaches its minimum only when $\rho_{\text{hss}} = 1/2$. In this case, the boundary is given by

$$V_c = \frac{\rho^2 + (1 - \rho)^2}{\rho(1 - \rho)}(t_1 + t_2), \quad \text{and}$$

$$\rho_c = \frac{1}{2}\left(1 - \sqrt{\frac{V - 2(t_1 + t_2)}{V + 2(t_1 + t_2)}}\right). \quad \text{(C8)}$$

The mean-field phase diagrams can then be obtained based on the above analysis, which are depicted in Fig. 13. When $t_2 = 0$, it has been shown that doping the crystal at $\rho = 1/2$ with additional holes or particles leads to the PS between the CB solid state and SF state. The presence of t_2 greatly suppresses the regime of this usual PS phase, where the HSS phase with additional PS* state between SF and HSS regimes appears on the top of the diagram. The boundary between the two different PS states is determined by $\widetilde{V}_c = -2(t_1 + t_2) - t_1^2/t_2$. Interestingly, at the mean-field level, such boundary also overlaps with the lower tip of the HSS phase at $\rho = 1/2$. We note that in the TNS results, this boundary shifts upwards, as shown in Fig. 1, which indicates that the mean-field calculation overestimates the lower boundary of $\widetilde{V}_c$. Moreover, the HSS states gradually dominate the phase diagram as $|t_2|$ approaches the highly frustrated point $|t_2| = t_1/2$, suggesting
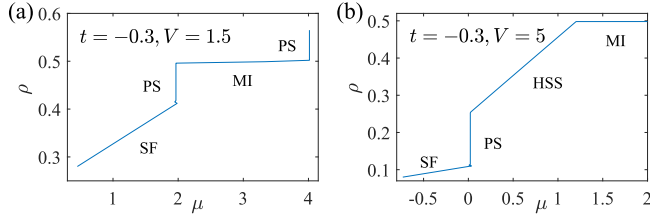
FIG. 14. ρ versus μ for fixed $t_2 = -0.3$ and different (a) $V = 1.5$ and (b) 5, respectively, in the hard-core limit. The vertical lines show the locations where phase separation occurs, which is similar to the curve obtained from the Maxwell construction for canonical ensembles.
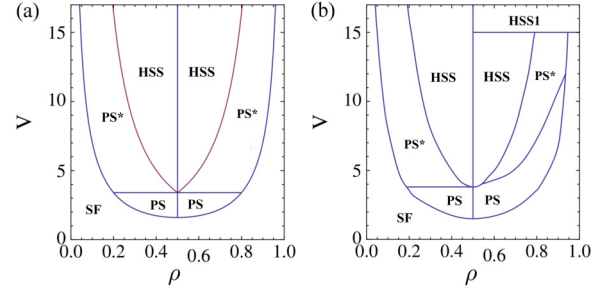

FIG. 15. Phase diagrams in the ρ-V plane for $t_2 = -0.2$ with different (a) $U = \infty$ and (b) $U = 60$. There are two different HSS state for $zV < U$ and $zV > U$, respectively, when $\rho > 1/2$.

that the SS state can be stabilized for arbitrary $\rho < 1/2$, which is unattainable in the usual Bose-Hubbard model without frustrated hopping.

We would like to note that although the above results are obtained within the constraints of fixed total particle numbers, the approximation based on the Gutzwiller wave function make it different from the usual particle-number-conserved system. In addition, the optimization procedure employed during the calculation also excludes the possibilities of finding uniform phases within the PS regime. To show this, we also plot the ρ-μ curves by sweeping ρ across the PS regime in Fig. 14. The appearance of vertical lines indicates that the whole system is the mixture of two different phases, similar to that obtained from the usual Maxwell construction for canonical ensembles.

3. Fate of SS state in the soft-core case

In the soft-core case, the breakdown of particle-hole symmetry around $\rho = 1/2$ results in different phases when the additional holes and bosons are introduced. For $\rho < 1/2$, the doped holes can hop within the occupied lattices to reduce the kinetic energy, which leads to the HSS phase and is very similar to the hard-core limit $U \to \infty$. When $\rho > 1/2$, the additional bosons can be placed on either sublattice. The system can be in different phases depending on the relative ratio of t_1, t_2, U, and zV, respectively.

Specifically, when $zV < U$, there are two different ways to lower the energy of the system. In the first case, the particles are located within the unoccupied sublattice, which can then hop to the NNN site due to the presence of t_2. This is a HSS state where superfluid exists only within one sublattice. The total energy gain per particle can be estimated as $\Delta E_2' = zV - 4|t_2|$. On the other hand, when the bosons can hop between the occupied and unoccupied sites, the energy gain is given by the lowest eigenvalue of the following coupling matrix as

$$\begin{pmatrix} U + 2z|t_2| & \sqrt{2}zt_1 \\ \sqrt{2}zt_1 & zV + z|t_2| \end{pmatrix} \quad \text{(C9)}$$

and reads

$$\Delta E_- = U + \Delta + 3z|t_2|/2 - \sqrt{2(zt_1)^2 + (z|t_2|/2 - \Delta)^2}, \quad \text{(C10)}$$

where $2\Delta = zV - U$. The ground-state configuration can then be determined by the difference

$$\delta E = \Delta E_- - \Delta E_2'$$
$$= -\Delta + 5z|t_2|/2 - \sqrt{2(zt_1)^2 + (z|t_2|/2 - \Delta)^2}, \quad \text{(C11)}$$

which corresponds to a HSS phase when $\Delta E_- > \Delta E_2'$, and a SS phase when $\Delta E_- < \Delta E_2'$. Many interesting features can be obtained from the above formula and we summarize them as follows.

(i) It is easy to check that for very small NNN hoppings $|t_2| \simeq 0$, we always have $\delta E = -\Delta - \sqrt{2(zt_1)^2 + \Delta^2} < 0$, therefore the SS phase is favored for all Δ when we dope the crystal at $\rho = 1/2$ with particles.

(ii) When $|\Delta| \gg \max(|t_1|, |t_2|)$, we find $\delta E \sim 8(|t_2| - 2t_1^2/|\Delta|) > 0$, which leads to the stabilization of HSS phase in this case. We note that in the hard-core limit, since $|\Delta| \to \infty$, such HSS phase is always more stable than the SS phase, and consistent with the previous discussion.

(iii) On the other side with $|\Delta| \sim 0$, we have $\delta E \sim 5z|t_2|/2 - \sqrt{2(zt_1)^2 + (z|t_2|/2)^2} < 0$ for all $|t_2| < t_1/2$. The ground state is described by a SS state.

(iv) The boundary between the SS phase and HSS phase can be estimated from $\delta E = 0$, which gives $|\Delta_c| = 2[(t_1/t_2)^2 - 3]|t_2|$.

The above arguments can also be extended to $zV > U$ with

$$\delta E = \Delta E_- - \Delta E_2''$$
$$= \Delta + 5z|t_2|/2 - \sqrt{2(zt_1)^2 + (z|t_2|/2 - \Delta)^2}, \quad \text{(C12)}$$

where $\Delta > 0$ and $\Delta E_2'' = U - 4|t_2|$ is the total energy of a single boson delocalized within the occupied sublattice due to t_2. In the case $|\Delta| \gg \max(|t_1|, |t_2|)$, we have $\delta E \sim 4(3|t_2| - 4t_1^2/|\Delta|) > 0$, which indicates that the HSS state is favored. When $\Delta \sim 0$, we still have $\delta E < 0$. Therefore, the SS state also exists only within a very smaller regimes around the $zV = U$. This is very different from the nonfrustrated case, where SS state is stabilized almost for all $zV > U$.

Figure 15(b) depicts the phase diagram in the ρ-V plane for $t_2 = -0.2$ with finite $U = 60$. Since $U \gg (|t_1|, |t_2|)$, the phase diagram is only slightly changed on the $\rho < 1/2$ side compared with the hard-core case [Fig. 2(a)]. When $\rho > 1/2$,

there are two HSS states on the different side of the critical line $zV = U$. When $zV > U$, all particles locate within one sublattice to reduce the interaction energy due to the presence of frustrated hoppings. This corresponds to the HSS1 state where the mean occupation number is larger than one. In the opposite case with $zV < U$, the additional particles take place the unoccupied lattice to form a sublattice SF state, while the remaining sublattice is still a CB solid state. Therefore, the whole system is composed of a uniform mixture of solid and SF states, which is the usual particle-hole counterpart of the HSS state in the regime $\rho < 1/2$. Similarly, the PS state between the HSS phase and SF phase can be viewed as the mixture of the two phases.

Further decreasing U makes it energetically more favorable for additional bosons hopping over both occupied and unoccupied sites. Such effect is very apparent when $|t_2| \ll t_1/2$, where the SS state dominates the phase diagram, as shown in Fig. 16. Meanwhile, an intermediate PS occurs between the SS and SF phases. When $|\Delta| \gg 0$, ΔE_- can be larger than ΔE_1 as increasing $|t_2|$. This leads to the stabilization of HSS and HSS1 phases for large $|\Delta|$. In addition, the regime of SS state shrinks and exists only around the critical point $zV = U$ above half filling.

The above mean-field results have also been checked by our numerical calculation using TNS. Comparatively speaking, the results suggest that the HSS phase above half filling is more fragile than that predicted based on such mean-field treatment. For the same parameters used in Fig. 16(b), the HSS phase is completely missing when $\rho > 1/2$, as shown in Fig. 4 in the main text. To show the competition between SS and HSS phase as we decrease the on-site interaction U, we also plot the transition points along with U for different ratios $zV/U = 0.5$ and 0.8 using TNS, as shown in Fig. 5. The results indicate that along with the decreasing of U, the SS phase appears first around $zV \sim U$, and dominates the phase
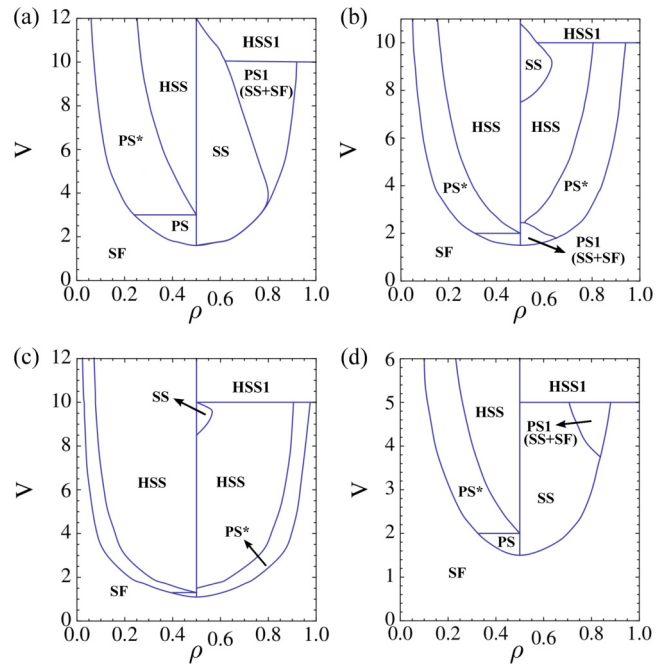

FIG. 16. Phase diagrams in the ρ-V plane for $U = 40$ with different (a) $t_2 = -0.2$, (b) $t_2 = -0.3$, and (c) $t_4 = -0.4$. The SS phase becomes more stable as decreasing the on-site interaction U. While the HSS state can be favored by increasing $|t_2|$, SS exists only within a relatively smaller regime around $zV = U$ by doping additional particles. (d) shows the phase diagram for $U = 20$ and $t_2 = -0.2$.

diagram as decreases, which is consistent with the above discussions. U We also note that no phase-separation regimes composed of the mixture of SS and SF phases are found during the TNS calculation.

[1] H. Diep, *Frustrated Spin Systems* (World Scientific, Singapore, 2013).

[2] P. W. Anderson, Mater. Res. Bull. **8**, 153 (1973).

[3] L. Balents, Nature (London) **464**, 199 (2010).

[4] G. Wannier, Phys. Rev. **79**, 357 (1950).

[5] P. W. Anderson, Science **235**, 1196 (1987).

[6] P. A. Lee, N. Nagaosa, and X.-G. Wen, Rev. Mod. Phys. **78**, 17 (2006).

[7] M. P. A. Fisher, P. B. Weichman, G. Grinstein, and D. S. Fisher, Phys. Rev. B **40**, 546 (1989).

[8] D. Jaksch, C. Bruder, J. I. Cirac, C. W. Gardiner, and P. Zoller, Phys. Rev. Lett. **81**, 3108 (1998).

[9] M. Lewenstein, A. Sanpera, V. Ahufinger, B. Damski, A. Sen, and U. Sen, Adv. Phys. **56**, 243 (2007).

[10] M. Greiner, O. Mandel, T. Esslinger, T. W. Hänsch, and I. Bloch, Nature (London) **415**, 39 (2002).

[11] J. Dalibard, F. Gerbier, G. Juzeliūnas, and P. Öhberg, Rev. Mod. Phys. **83**, 1523 (2011).

[12] G. Möller and N. R. Cooper, Phys. Rev. A **82**, 063625 (2010).

[13] S. D. Huber and E. Altman, Phys. Rev. B **82**, 184502 (2010).

[14] S. Powell, R. Barnett, R. Sensarma, and S. D. Sarma, Phys. Rev. A **83**, 013612 (2011).

[15] S. Inglis and R. G. Melko, New J. Phys. **13**, 053018 (2011).

[16] A. Dhar, M. Maji, T. Mishra, R. V. Pai, S. Mukerjee, and A. Paramekanti, Phys. Rev. A **85**, 041602 (2012).

[17] Y.-Z. You, Z. Chen, X.-Q. Sun, and H. Zhai, Phys. Rev. Lett. **109**, 265302 (2012).

[18] Y. Chan and L. Duan, New J. Phys. **14**, 113039 (2012).

[19] A. Dhar, T. Mishra, M. Maji, R. V. Pai, S. Mukerjee, and A. Paramekanti, Phys. Rev. B **87**, 174501 (2013).

[20] T. Mishra, S. Greschner, and L. Santos, Phys. Rev. B **92**, 195149 (2015).

[21] G. Zhu, J. Koch, and I. Martin, Phys. Rev. B **93**, 144508 (2016).

[22] X.-F. Zhou, Z.-X. Chen, Z.-W. Zhou, Y.-S. Zhang, and G.-C. Guo, Phys. Rev. A **81**, 021602 (2010).

[23] Z.-X. Chen, H. Ma, M.-H. Chen, X.-F. Zhou, L. He, G.-C. Guo, X. Zhou, Y. Chen, and Z.-W. Zhou, Phys. Rev. A **85**, 013632 (2012).

[24] A. F. Andreev and I. M. Lifshitz, Sov. Phys. JETP **29**, 1107 (1969).

[25] G. Chester, Phys. Rev. A **2**, 256 (1970).

[26] A. J. Leggett, Phys. Rev. Lett. **25**, 1543 (1970).

[27] D. Y. Kim and M. H. W. Chan, Phys. Rev. Lett. **109**, 155301 (2012).

[28] T. Lahaye, C. Menotti, L. Santos, M. Lewenstein, and T. Pfau, Rep. Prog. Phys. **72**, 126401 (2009).

[29] A. Griesmaier, J. Werner, S. Hensler, J. Stuhler, and T. Pfau, Phys. Rev. Lett. **94**, 160401 (2005).

[30] M. Lu, N. Q. Burdick, S. H. Youn, and B. L. Lev, Phys. Rev. Lett. **107**, 190401 (2011).

[31] K. Aikawa, A. Frisch, M. Mark, S. Baier, A. Rietzler, R. Grimm, and F. Ferlaino, Phys. Rev. Lett. **108**, 210401 (2012).

[32] M. Boninsegni and N. Prokof'ev, Phys. Rev. Lett. **95**, 237204 (2005).

[33] R. G. Melko, A. Paramekanti, A. A. Burkov, A. Vishwanath, D. N. Sheng, and L. Balents, Phys. Rev. Lett. **95**, 127207 (2005).

[34] D. Heidarian and K. Damle, Phys. Rev. Lett. **95**, 127206 (2005).

[35] G. G. Batrouni, R. T. Scalettar, G. T. Zimanyi, and A. P. Kampf, Phys. Rev. Lett. **74**, 2527 (1995).

[36] G. G. Batrouni and R. T. Scalettar, Phys. Rev. Lett. **84**, 1599 (2000).

[37] P. Sengupta, L. P. Pryadko, F. Alet, M. Troyer, and G. Schmid, Phys. Rev. Lett. **94**, 207202 (2005).

[38] B. Capogrosso-Sansone, C. Trefzger, M. Lewenstein, P. Zoller, and G. Pupillo, Phys. Rev. Lett. **104**, 125301 (2010).

[39] T. Ohgoe, T. Suzuki, and N. Kawashima, Phys. Rev. B **86**, 054520 (2012).

[40] K. P. Schmidt, J. Dorier, A. M. Läuchli, and F. Mila, Phys. Rev. Lett. **100**, 090401 (2008).

[41] Y.-C. Chen, R. G. Melko, S. Wessel, and Y.-J. Kao, Phys. Rev. B **77**, 014524 (2008).

[42] Y.-H. Chan, Y.-J. Han, and L.-M. Duan, Phys. Rev. A **82**, 053607 (2010).

[43] T. Ohgoe, T. Suzuki, and N. Kawashima, Phys. Rev. A **86**, 063635 (2012).

[44] T. Ying, G. G. Batrouni, V. G. Rousseau, M. Jarrell, J. Moreno, X. D. Sun, and R. T. Scalettar, Phys. Rev. B **87**, 195142 (2013).

[45] F. Wang, F. Pollmann, and A. Vishwanath, Phys. Rev. Lett. **102**, 017203 (2009).

[46] R. Sachdeva and S. Ghosh, Phys. Rev. A **85**, 013642 (2012).

[47] Y.-F. Wang, Z.-C. Gu, C.-D. Gong, and D. N. Sheng, Phys. Rev. Lett. **107**, 146803 (2011).

[48] G. Vidal, Phys. Rev. Lett. **91**, 147902 (2003).

[49] F. Verstraete and J. I. Cirac, cond-mat/0407066.

[50] N. Schuch, M. M. Wolf, F. Verstraete, and J. I. Cirac, Phys. Rev. Lett. **100**, 040501 (2008).

[51] W. Liu, C. Wang, Y. Li, Y. Lao, Y. Han, G.-C. Guo, and L. He, J. Phys.: Condens. Matter. **27**, 085601 (2015).

[52] G. Vidal, Phys. Rev. Lett. **93**, 040502 (2004).

[53] M. Fannes, B. Nachtergaele, and R. Werner, Commun. Math. Phys. **144**, 443 (1992).

[54] G. Vidal, Phys. Rev. Lett. **99**, 220405 (2007).

[55] Z. Wang, Y. Han, G.-C. Guo, and L. He, Phys. Rev. B **88**, 121105(R) (2013).

[56] R. H. Swendsen and J.-S. Wang, Phys. Rev. Lett. **57**, 2607 (1986).

[57] C. J. Geyer, in *Computer Science and Statistics, in Proceedings of the 23rd Symposium on the Interface* (Interface Foundation, Fairfax Station, 1991).

[58] T. Kimura, Phys. Rev. A **84**, 063630 (2011).